Modeling and control of a waste heat recovery system for integrated powertrain design optimization

Available online at www.sciencedirect.com

ScienceDirect

IFAC PapersOnline CONFERENCE PAPER ARCHIVE

IFAC PapersOnLine 52-5 (2019) 598–603

Modeling and control of a waste heat recovery system for integrated powertrain design optimization

K. Kruijt * **F.J.R. Verbruggen** * **M.F.M. Speetjens** * **T. Hofman** *

* *Eindhoven University of Technology, Den Dolech 2, 5600 MB, The Netherlands (e-mail: k.kruijt@student.tue.nl; f.j.r.verbruggen@tue.nl; m.f.m.speetjens@tue.nl; t.hofman@tue.nl).*

Abstract: The growing demand for increased vehicle efficiency has led to the introduction of waste heat recovery techniques in vehicle powertrains, with the organic Rankine cycle as the most interesting technique for automotive applications. In order to integrate the design of the waste heat recovery system into the design optimization of the full powertain, a novel modeling approach is suggested for capturing the key dynamics of a waste heat recovery system with low computational effort and number of design parameters, and which is scalable with the individual components of the cycle. The model is compared with a detailed finite volume model for a given organic Rankine cycle. Secondly, the organic Rankine cycle is integrated into a parallel hybrid vehicle model, and an optimization routine is proposed for obtaining the optimal control trajectories for the powertrain over a drive cycle. The main purpose of the waste heat recovery model designed in this paper in combination with the proposed optimization algorithm is to be used for powertrain design optimization studies.

Keywords: Organic Rankine Cycle, Hybrid Vehicles, Optimization, Optimal Control, Modelling

1. INTRODUCTION

In the last decades, the number of electrified vehicles on the road has increased. Despite this growing trend of electrified vehicles, the internal combustion engine (ICE) will remain essential for conventional and hybrid vehicles. In order to improve the efficiency of the ICE, new technologies have been introduced, such as turbo-charging, alternative fuels, etc. To further improve fuel efficiency, without negatively affecting emissions, waste heat recovery (WHR) is a promising solution. Different WHR techniques exist (Lion et al., 2017a), though for automotive applications the organic Rankine cycle (ORC) seems the most promising candidate. The potential for fuel economy savings of ORC technology varies strongly with the application and configuration, but has an expected fuel saving potential of up to 10% for heavy-duty vehicles (Lion et al., 2017b).

In order to find the optimal design for the powertrain of a vehicle, all powertrain components need to be taken into account. This is often referred to as integrated powertrain design. However, typically the design of a WHR system is exclusively based on an already existing powertrain configuration, and does not integrate the WHR design with the design of the rest of the powertrain. Only a limited number of studies (Petr et al., 2017; Zhao et al., 2018) seek improvement in the overall powertrain efficiency, by integrating the design of the WHR system with the design of the rest of the powertrain.

In order to perform an integrated powertrain design optimization, a model of the ORC system is required. Most used modeling techniques for ORC system design are finite volume (FV) models (Chowdhury et al., 2015) and moving boundary (MB) models (Peralez et al., 2013; Huster et al., 2018). The main purpose of these models is to be used for control optimization of the ORC system. However, these techniques are unattractive for design optimization of the full powertrain, as they require a higher computational effort and a large set of parameters to characterize the system. This is unwanted for powertrain design studies where a large number of simulations have to be run, and where each extra design variable quickly increases the design space and thereby computational expenses. More suitable modeling approaches focus on capturing the steady-state behavior of an ORC by applying look-up maps or pinch diagram analysis (Rosset et al., 2018). However, these models leave out the dynamics of the system that play an important role in ORC applications in vehicles for which highly transient drive cycles are generally compelled. Thus, an ORC model used for the purpose of powertrain design optimization requires to have a good trade-off between accuracy (and describing the systems dynamics) and computational efficiency.

Therefore, the proposed dynamic ORC model in this paper consists of an expansion of the standard thermodynamic model of a Rankine cycle so as to include instationary effects. This is essential to adequately describe the main dynamics of the ORC system, which are required for powertrain design optimization. The standard model includes four basic thermodynamic processes involved in a phase-change power cycle (compression, evaporation, expansion, condensation) and admits full description by four thermo-

10.1016/j.ifacol.2019.09.095

dynamic states separating these processes. The dynamic ORC model has the same structure yet with expanded relations for the thermodynamic states that account for transient behavior. The ORC model is compared with a more detailed ORC model, which is based on a FV approach (Chowdhury et al., 2015). Next, to make the model suitable for powertrain design optimization, this paper describes an optimal control approach for obtaining the control input of a parallel hybrid powertrain configuration. This approach combines equivalent minimization consumption strategy (ECMS) with a Newton-Raphson shooting method, which secures a charge sustaining strategy.

In the remainder of this paper, Section 2 describes the working principle of an ORC. Subsequently, in Section 3, the dynamic ORC model is described, followed by a comparison of the model with a FV model in Section 4. In Section 5, the ORC model is integrated into powertrain model of a parallel hybrid heavy-duty truck, for which in Section 6 the optimal control problem with the WHR integrated in the powertrain is described. Section 7 elaborates on the optimization results followed by the conclusion in Section 8.

2. ORGANIC RANKINE CYCLE PRINCIPLE

The ORC system in vehicles mostly obtains heat from the tailpipe, or from the exhaust gas recirculation (EGR) system. The ORC, graphically illustrated in Fig. 1, goes through different phases in order to convert waste heat into mechanical power at the output of the turbine. However, also electric power can be recovered, by coupling an electric machine (EM) to the output of the turbine. In this paper an ORC cycle without recuperator is studied, and only the tailpipe is used as heat source.

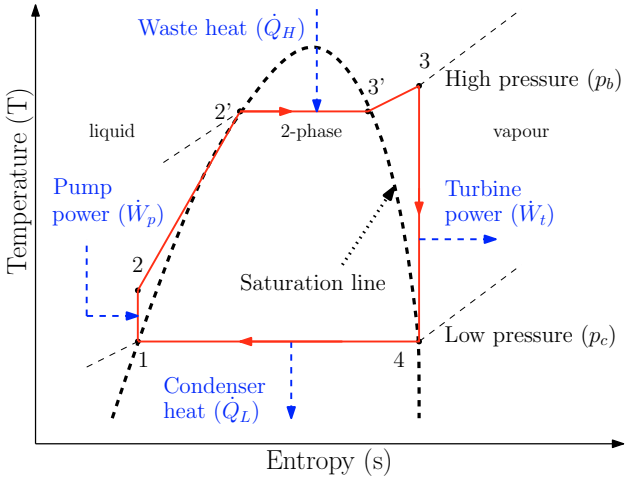

Fig. 1. Temperature-entropy diagram of an organic Rankine cycle

The cycle is determined by two operating pressures, boiler side p_b and condenser side p_c. From the saturated low pressure side, a liquid $\langle 1 \rangle$ flows through a pump, that increases the medium to a saturated high pressure $\langle 2 \rangle$. Secondly, the medium passes through the boiler and goes through a phase change from saturated liquid $\langle 2' \rangle$ to dry vapor $\langle 3' \rangle$, whereby the fluid is superheated $\langle 3 \rangle$. In the boiler heat is extracted from the exhaust gases in order to heat up the medium. Subsequently, the superheated vapor enters the expander, whereby the medium expands and work is extracted. A low pressure gas remains $\langle 4 \rangle$, which eventually, via the condenser, is cooled and condensed back to a saturated liquid $\langle 1 \rangle$. The individual components of the ORC system, are denoted as, pump (*"p"*), boiler (*"b"*), turbine (*"t"*) and condenser (*"c"*). Next to this, the positions (1, 2, 3, 4) respectively comprehend the locations in-between the components (as illustrated in Fig. 2).

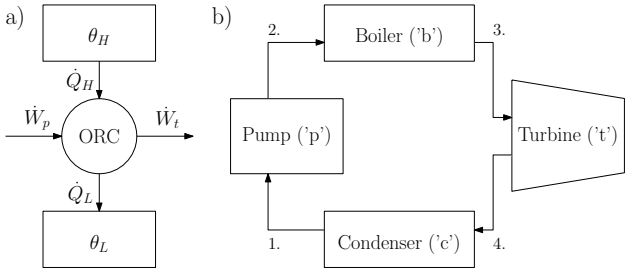

Fig. 2. (a) Standard dynamic organic Rankine cycle (b) and configuration with main components

3. MODELING OF THE ORGANIC RANKINE CYCLE

The ORC model is derived by assuming a constant mass flux within the control volume (cv). Direct derivation is possible of the governing equations from First and Second law of thermodynamics (Turns, 2006)

$$\left.\frac{\mathrm{d}U}{\mathrm{d}t}\right|_{cv} = \dot{Q} - \dot{W} + \dot{m}_o\,(h_{in} - h_{out}), \tag{1}$$

$$\left.\frac{\mathrm{d}S}{\mathrm{d}t}\right|_{cv} = \int_\Gamma \frac{\delta\dot{Q}}{\theta} + \dot{m}_o\,(s_{in} - s_{out}) + \dot{S}_*. \tag{2}$$

The pump $\langle 1 \rangle - \langle 2 \rangle$ and the turbine $\langle 3 \rangle - \langle 4 \rangle$ are assumed as ideal processes, i.e., reversible (entropy production: $\dot{S}_* = 0$) and adiabatic (cyclic integral: $\int_\Gamma \frac{\delta\dot{Q}}{\theta} = 0$). The boiler and condenser are assumed to be isobaric ($\dot{W} = 0$) and exchange heat on basis of the difference between the reservoir temperatures ($\theta_H = \theta_H(t)$ and $\theta_L = \theta_L(t)$) and the mean boiler and condenser temperatures ($\overline{\theta}_b$ and $\overline{\theta}_c$). All four of these temperatures can vary over time. The massflow is assumed constant ($\dot{m}_{in} = \dot{m}_{out} = \dot{m}_o$). The resulting heat exchange $\dot{Q}$, as part of (1)-(2) can be calculated with

$$\dot{Q}_H = \kappa_b\, A_b\, (\theta_H - \overline{\theta}_b), \tag{3}$$

$$\dot{Q}_L = \kappa_c\, A_c\, (\theta_L - \overline{\theta}_c). \tag{4}$$

Parameters κ and A are the heat-transfer coefficient and heat-transfer area, respectively.

To solve (1)-(2), the actual state within the components is estimated by a weighted average α over the inlet and outlet state of the component. These α's are calibration parameters, and can be used to fit the model to an existing system. For example, to compute the specific enthalpy h inside the pump,

$$h_p = \alpha_p \cdot h_1 + (1 - \alpha_p) \cdot h_2. \tag{5}$$

Implementing the assumptions mentioned above into the First and Second law of thermodynamics (1)-(2) and making the choice to use entropy as the state, each of

the components can be described by only one of the laws, resulting in a compact model. The following models are used for each of the components,

$$\alpha_p \frac{\mathrm{d}s_1}{\mathrm{d}t} + (1-\alpha_p)\frac{\mathrm{d}s_2}{\mathrm{d}t} = \frac{1}{\tau_p}(s_1 - s_2), \tag{6}$$

$$\alpha_t \frac{\mathrm{d}s_3}{\mathrm{d}t} + (1-\alpha_t)\frac{\mathrm{d}s_4}{\mathrm{d}t} = \frac{1}{\tau_t}(s_3 - s_4), \tag{7}$$

$$\gamma_2\,\alpha_b \frac{\mathrm{d}s_2}{\mathrm{d}t} + \gamma_3\,(1-\alpha_b)\frac{\mathrm{d}s_3}{\mathrm{d}t} = \frac{1}{\tau_b}\,(h(s_2|_{p_b}) - h(s_3|_{p_b})) + \beta_b\left(\theta_H - (\alpha_b\,\theta(s_2|_{p_b}) + (1-\alpha_b)\,\theta(s_3|_{p_b}))\right), \tag{8}$$

$$\gamma_4\,\alpha_c \frac{\mathrm{d}s_4}{\mathrm{d}t} + \gamma_1\,(1-\alpha_c)\frac{\mathrm{d}s_1}{\mathrm{d}t} = \frac{1}{\tau_c}\,(h(s_4|_{p_c}) - h(s_1|_{p_c})) + \beta_c\left(\theta_L - (\alpha_c\,\theta(s_4|_{p_c}) + (1-\alpha_c)\,\theta(s_1|_{p_c}))\right). \tag{9}$$

Here $s_i|_p$ indicates s_i at given pressure p. The coefficients used in (6)-(9),

$$\gamma_i = \frac{\partial u_i}{\partial s_i}\Big|_p, \quad \tau_j = \frac{m_j}{\dot{m}_o}, \quad \beta_j = \frac{\kappa_j\,A_j}{m_j}, \tag{10}$$

with $i \in \{1,2,3,4\}$ and $j \in \{p,b,t,c\}$. The temperature θ, internal energy u and enthalpy h are numerically available by the CoolProp library (Bell et al., 2013), for a variety of fluids. The partial derivative of internal energy with respect to entropy at constant pressure is written as $\frac{\partial u_i}{\partial s_i}|_p$, and the mass content of working fluid in each of the four components is denoted by m_j.

3.1 State space model

Alternatively, we can express equations (6)-(9) in state-space form

$$S\frac{\mathrm{d}\boldsymbol{s}}{\mathrm{d}t} = B\boldsymbol{s} + C\boldsymbol{\theta}(\boldsymbol{s}|_{p_b,p_c}) + D\boldsymbol{h}(\boldsymbol{s}|_{p_b,p_c}) + E\boldsymbol{z}(t). \tag{11}$$

Here bold symbols indicate vectors. The input vector $\boldsymbol{z}$ contains the reservoir temperatures: $\boldsymbol{z} = [\theta_H(t)\ \ \theta_L(t)]$. By using semi-implicit Euler time integration (Cellier and Kofman, 2006), numerical simulation of the evolution over time Δt of the state vector $\boldsymbol{s} = [s_1\, s_2\, s_3\, s_4]$ is possible

$$\boldsymbol{s}_{n+1} = Q\,(S\,\boldsymbol{s}_n + \Delta t\,\boldsymbol{F}), \tag{12}$$

where

$$Q = (S - \Delta t\,B)^{-1}, \tag{13}$$

$$\boldsymbol{F} = C\,\boldsymbol{\theta}(\boldsymbol{s_n}|_{p_b,p_c}) + D\,\boldsymbol{h}(\boldsymbol{s}_n|_{p_b,p_c}) + E\,\boldsymbol{z}_{n+1}. \tag{14}$$

Here B, C, D, E and S in (11)-(14) are denoted as the system matrices.

3.2 Steam quality penalty

To prevent damage to the turbine blades, often a by-pass is used which only allows steam to enter the expander. To capture this in the model, a penalty p_χ is added,

$$p_\chi = \min\left(1,\ \frac{u_3}{u_{g|_{p_b}}}\right)^k, \tag{15}$$

with exponent $k = 70$ and $u_{g|_{p_b}}$ represents the internal energy at the saturated line of vapor at pressure p_b.

Combining (12-14) with the penalty from (15), the work exchanges in pump $\dot{W}_p$ and turbine $\dot{W}_t$ can be calculated by

$$\dot{W}_p = \dot{m}_o\,(h(s_1|_{p_c}) - h(s_2|_{p_b})) - m_p\left(\gamma_1\,\alpha_p\frac{\mathrm{d}s_1}{\mathrm{d}t} + \gamma_2\,(1-\alpha_p)\frac{\mathrm{d}s_2}{\mathrm{d}t}\right), \tag{16}$$

$$\dot{W}_t = p_\chi\left(\dot{m}_o\,(h(s_3|_{p_b}) - h(s_4|_{p_c})) - m_t\left(\gamma_3\,\alpha_t\frac{\mathrm{d}s_3}{\mathrm{d}t} + \gamma_4\,(1-\alpha_t)\frac{\mathrm{d}s_4}{\mathrm{d}t}\right)\right). \tag{17}$$

The flow being by-passed is expanded over an expansion valve.

3.3 Complete waste heat recovery model

With the ORC modeling principle, as explained in previous sections, a WHR submodel can be created, which has inputs θ_H and θ_L and outputs $\dot{W}_t$, $\dot{W}_p$ and P_{fa}. The input-output schematic is illustrated in Fig. 3.

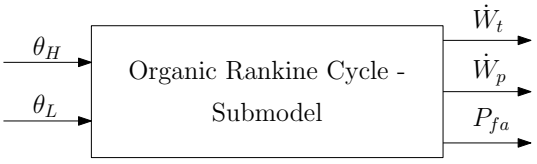

Fig. 3. Input-output diagram of the ORC submodel

For the high temperature θ_H the temperature of the exhaust gases from the ICE is used and θ_L the temperature in the cooling circuit. The exhaust gas temperature θ_H is determined using a look-up map,

$$\theta_H = f_1(T_e, \omega_e), \tag{18}$$

where T_e and ω_e are the torque and the rotational speed of the ICE. The lower reservoir temperature θ_L is assumed to be constant at 293 K.

The outputs of the submodel together represent the WHR output power P_w,

$$P_w = \eta_m \dot{W}_t + \dot{W}_p, \tag{19}$$

here the efficiency of the electric machine connected to the turbine η_m is taken into account. The mechanical pump power $\dot{W}_p$ yields negative values, as the component consumes power.

The output P_{fa} represent the consumption of the fan to cool the condenser of the WHR system, which is based upon simplified expressions of the condenser cooling $\dot{Q}_L$. P_{fa} is negative, as the component consume power.

4. COMPARISON OF ORGANIC RANKINE CYCLE MODELS

No comparison could be made with experimental ORC data, because of the unavailability of experimental data. Therefore, to create at least some insight in the performance of the ORC model, a comparison was made with a more detailed model (Chowdhury et al., 2015), which uses an FV model for the boiler. Therefore, the response in specific enthalpy h_3 at the outlet of the boiler is compared,

which is done by a step in the mass flow rate $\dot{m}_o$ from 0.25 kg/s to 0.1 kg/s (see Fig. 4). In the comparison, the initial conditions and parameters from (Chowdhury et al., 2015) are used, which are represented in Table 1.

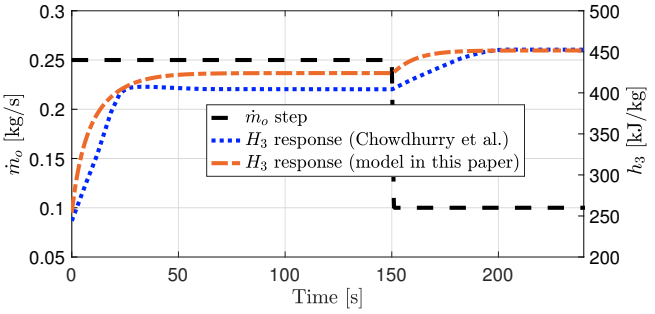

Fig. 4. Comparison of specific enthalpy h_3 response on a step in mass flow rate $\dot{m}_o$ with (Chowdhury et al., 2015).

Globally, both models follow a similar trend, however it can be observed that differences exists in the response. The observed differences are likely attributed to the differences in heat-transfer coefficient techniques as the ORC model in this paper assumes only a constant value for this.

Table 1. Configuration of ORC for comparison with (Chowdhury et al., 2015).

Configuration	Symbol	Value
Fluid in ORC cycle	–	R134a
Heat transfer area	A_b, A_c	5.78 m^2
Mass of boiler (estimated)	m_b	16 kg
Initial mass flow rate in ORC	$\dot{m}_o$	0.25 kg/s
Initial temperate of ORC	θ_1, θ_2, θ_3, θ_4	303 K
Temperature of heat source	θ_H	523 K
Pressure at boiler side	p_b	6 MPa

5. PARALLEL HYBRID VEHICLE MODEL WITH WASTE HEAT RECOVERY

The WHR model is integrated in a backwards facing simulation model of a parallel (p2) hybrid heavy-duty truck. Fig. 5 depicts the powertrain configuration, whereby the WHR system is added. The vehicle has a CE with maximum power of 330 kW, an EM with a maximum power of 150 kW, a 17.8 kWh battery, and a 12-speed gearbox.

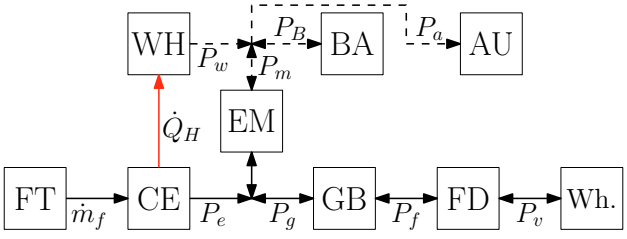

Fig. 5. Parallel hybrid powertrain topology with WHR (FT: fuel tank, CE: internal combustion engine, WH: waste heat recovery system, BA: battery, EM: electric machine, GB: gear-box, FD: final drive, AU: auxiliaries, Wh: wheels)

A small ORC configuratution is chosen with R245fa as fluid. The sizing of the ORC configuration is provided in Table 2.

Table 2. WHR sizing used with UDDS cycle.

Parameter	Symbol	Size
Fluid	-	R245fa
Size of boiler	A_b	0.8 m^2
Size of condenser	A_c	0.8 m^2
Mass content turbine	m_t	14 kg
Mass content pump	m_p	7 kg
Mass flow rate	$\dot{m}_o$	0.1 kg/s
Initial temperate of ORC	θ_1, θ_2, θ_3, θ_4	293 K
High pressure	p_b	30 bar
Model weighing parameters	$\alpha_1, \alpha_2, \alpha_3, \alpha_4$	0.1,0.3,0.05,0.05
WHR EM efficiency	η_m	0.8
Heat-transfer coefficient	κ_b	1000 W/m^2K
Heat-transfer coefficient	κ_c	1500 W/m^2K

5.1 Transmission model and torque-split

A simple transmission model is considered with an automated manual transmission (AMT). The final drive is modelled as a fixed efficiency η_{fd} and the efficiency in the gearbox η_g is gear-dependent, but fixed per gear x_g,

$$T_g = \begin{cases} \dfrac{T_v}{\eta_{fd}\,\eta_g(x_g)\,r_{fd}\,r_g(x_g)} & \text{if } T_v > 0, \\ \dfrac{\eta_{fd}\,\eta_g(x_g)\,T_v}{r_{fd}\,r_g(x_g)} & \text{if } T_v \leq 0. \end{cases} \tag{20}$$

For positive torque requests at the wheel ($T_v > 0$) and ($T_v \leq 0$) for negative torque requests, with the gearbox power P_g being

$$P_g = T_g\,\omega_g. \tag{21}$$

Moreover, a torque-split u_{ts} is taken into account, which divides the total torque at the gearbox T_g to torque demand from the EM, T_m, and the ICE, T_e,

$$T_e = (1 - u_{ts})\,T_g + T_{ma}, \tag{22}$$

$$T_m = \begin{cases} u_{ts}\,T_g & \text{if } T_g > 0 \\ (1 - u_{ts})\,T_g & \text{if } T_g \leq 0, \end{cases} \tag{23}$$

where T_{ma} is denoted as the torque coming from the mechanical auxiliaries, including, the alternator, oil pump and power steering.

5.2 Internal combustion engine and electric machine

The mass flow rate of fuel $\dot{m}_f$ and EM power P_m are calculated by using a steady-state look-up map,

$$\dot{m}_f = f_2(T_e, \omega_e), \tag{24}$$

$$P_m = f_3(T_m, \omega_m). \tag{25}$$

The inverter losses are included in (25).

5.3 Battery model

The battery is modeled using a equivalent circuit model. The battery open circuit voltage V_{oc} and internal resistance R are a function of the state of charge ξ of the battery

$$V_{oc} = f_4(\xi), \quad R = f_5(\xi). \tag{26}$$

The battery current I_B is calculated using

$$I_B = \frac{\eta_C\,(V_{oc} - \sqrt{{V_{oc}}^2 - 4\,R\,P_B})}{2\,R}, \tag{27}$$

where η_C is the coulomb efficiency. Furthermore, P_B represent the power flow on the high voltage bus,

$$P_B = P_a + P_m - P_w + P_{fa}, \tag{28}$$

where P_a is the electrical auxiliary power.

6. OPTIMAL CONTROL PROBLEM

In the optimal control problem, the control input vector $\boldsymbol{u}$ and state vector $\boldsymbol{x}$,

$$\boldsymbol{u}(t) = [u_{ts}(t)\ u_g(t)]^T, \tag{29}$$

$$\boldsymbol{x}(t) = [\xi(t)\ x_g(t)\ s_1(t)\ s_2(t)\ s_3(t)\ s_4(t)]^T, \tag{30}$$

are used to minimize equivalent fuel consumption $\dot{m}_{eq}$. The optimal control problem, with corresponding cost function J and constraints h_i, g_i, can be written as,

$$\begin{aligned}
\min_{\boldsymbol{u}} J(\boldsymbol{x}(t), \boldsymbol{u}(t), \Lambda(t)) &= \int_{t_0}^{t_f} \dot{m}_{eq}(\boldsymbol{x}(t), \boldsymbol{u}(t), \Lambda(t))\mathrm{dt}, \\
\text{s.t.} \quad \dot{x}(t) &= f(\boldsymbol{x}(t), \boldsymbol{u}(t), t), \\
h_{1,2}: \quad \xi(t_0) &= \xi(t_f) = \xi_0, \\
g_{3,4}: \quad -1 &\leq u_{ts} \leq 1, \\
g_{4,5}: \quad -I_B^{min} &\leq I_B(u_{ts}, x_g) \leq I_B^{max}, \\
g_{6,7}: \quad T_e^{min} &\leq T_e(u_{ts}, x_g) \leq T_e^{max}, \\
g_{8,9}: \quad \omega_e^{min} &\leq \omega_e(u_{ts}, x_g) \leq \omega_e^{max}, \\
g_{10,11}: \quad T_m^{min} &\leq T_m(u_{ts}, x_g) \leq T_m^{max}, \\
g_{12,13}: \quad \omega_m^{min} &\leq \omega_m(u_{ts}, x_g) \leq \omega_m^{max}.
\end{aligned} \tag{31}$$

with upper and lower boundaries (e.g. for battery current noted with superscripts min and max: I_B^{min} and I_B^{max}), the gear number x_g, the state of charge ξ of the battery, the torque-split u_{ts} and the gear-shift command u_g. The gear position $x_g \in \{1, 2, \ldots, 12\}$ is calculated as,

$$x_g(t) = x_g(t-1) + u_g(t), \tag{32}$$

with the discrete gear shift $u_g = \{-1, 0, 1\}$. Here -1 denotes a downshift, 1 a upshift and 0 when the gear is sustained. The drive cycle is denoted as $\Lambda(t)$, which consists of a velocity $v(t)$ and the slope $\phi(t)$ profile.

6.1 Heuristic optimal control

ECMS (Guzzella and Sciaretta, 2007) is applied to solve the optimal control problem, inspired by Pontryagin's Minimum Principle (PMP) formulation. Formally, PMP derivation requires for every state a co-state (Maamria, 2015). In this paper this is simplified and only one co-state is adopted within the Hamiltonian $\mathcal{H}$, given by,

$$\mathcal{H}(\boldsymbol{u}(t), \boldsymbol{x}(t)) = \dot{m}_f(\boldsymbol{u}(t), x_g(t)) + \lambda(t) \cdot \frac{\partial \xi}{\partial t} + p_g \cdot |u_g|^T, \tag{33}$$

where $\lambda(t)$ is the co-state. Moreover, a gear-shift penalty p_g was added to penalize frequent gear-shifting. A constant value of $p_g = 1e^{-4}$ [kg/s] provides a good balance between frequent gear-shifting and comfortable driving. With (33) the optimal control trajectory $u^*(t)$ is obtained,

$$\boldsymbol{u}^*(t) = \arg\min_{\boldsymbol{u} \in U} \mathcal{H}(\boldsymbol{u}(t), \boldsymbol{x}(t)), \tag{34}$$

by minimizing the Hamiltonian $\mathcal{H}$ for each time instant.

6.2 Newton-Raphson shooting method

At initial t_0 and final time t_f, the equality constraint $h_{1,2}$ (31) needs to hold, hence the parallel hybrid configuration needs to maintain a charge sustaining strategy. This is achieved by tuning λ, which is a constant value over the drive cycle. By doing so, battery usage can either be favored (by selecting lower values for λ) or discouraged (by selecting higher values for λ). To obtain a value for λ that satisfies the terminal constraint ($\xi(t_f) = \xi_f$), the Newton-Raphson shooting approach is deployed,

$$\lambda_{k+1} = \lambda_k + \frac{\Delta\lambda}{\Delta\xi(t_f)}(\xi_f - \xi(t_f)) \text{ with } k \in \{1, 2, \ldots, n\}, \tag{35}$$

whereby k is the number of the shooting attempt, and $\frac{\Delta\lambda}{\Delta\xi(t_f)}$ is actively re-calibrated with the best two shooting attempts. One shooting attempt means running the drive cycle once. In order to converge to a charge sustaining solution, usually three up to five shooting attempts are required. The routine is illustrated in Fig. 6 for the urban dynamometer driving schedule (UDDS).

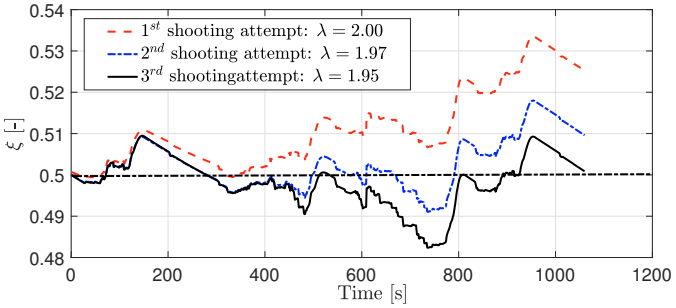

Fig. 6. Newton-Raphson shooting method to secure charge sustaining on UDDS drive cycle.

7. SIMULATION RESULTS OF OPTIMAL CONTROL TRAJECTORY

Given the configuration as mentioned in Table 2, the optimal control is solved by the ECMS routine [1] over the UDDS drive-cycle, which is 8.9 km long. The results of the WHR power P_w, the optimal trajectory for the gear position x_g^*, and the difference in optimal trajectory for the torque split between the vehicle with WHR $u_{ts,w}^*$ and the baseline vehicle $u_{ts,b}^*$, are shown in Fig. 7.

The upper figure of Fig. 7 shows that the WHR systems needs some time to warm up before starting to produce power, which at maximum goes up to 8 kW. The presence of a WHR system, increases the availability of electrical energy and favors the use of the EM, hence the higher values for the torque split when a WHR system is present $u_{ts,w}^*$. Another interesting observation is that higher gears are favored when including a WHR system. A possible explanation for this is that higher gears have a higher efficiency but also lead to higher torques at the ICE. Due to the presence of a WHR system, the EM has more electrical energy available to reduce the torque at the ICE, so that a higher gear can be chosen. The total benefit of adding the WHR system for this particular vehicle on this drive cycle, under the assumptions made in Section 3, is a 2,5% improvement in fuel economy.

Simulations are also run on a more highway type of drive cycle with a length of 100 km. Here, similar observations are seen, however, on this cycle is also clearly seen that the

[1] Total simulation time was 34.2 seconds with a 2.2 Ghz Intel Core i7 and 8 GB RAM using MATLAB R2016B. Four shooting attempts were required to converge to a charge sustaining solution.

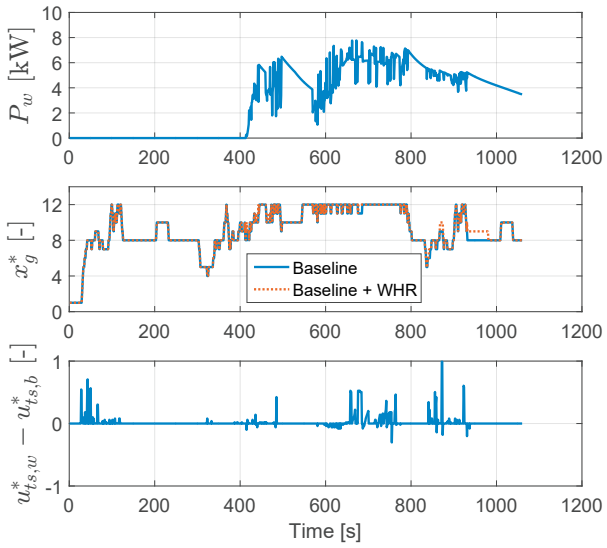

Fig. 7. WHR power P_w and optimal trajectory for the gear position x_g^*, and difference in optimal trajectory of torque split between vehicle with WHR $u_{ts,w}^*$ and the baseline vehicle $u_{ts,b}^*$ over the UDDS cycle.

configuration with WHR requires less charging ($u_{ts} < 0$) by the ICE, because of the WHR that on average produces 5.5 kW. On this highway cycle a 6 % improvement in fuel economy is calculated. In other literature, fuel savings in the range of 2.7 - 7.5 % have been calculated for highway driving for trucks (Lion et al., 2017a), 3.5 % by (Feru et al., 2016), and 5.1 - 6.0 % (Stanton, 2013). However, these systems use heat from both the EGR system as the exhaust. Exhaust only WHR shows fuel savings more in the range of 2 % (Nelson, 2008). Thus, the results found are rather high for an exhaust only WHR case. This might be related to the assumption of an ideal turbine.

8. CONCLUSION

The goal was to create a waste heat recovery model, with low computational expenses and number of model parameters, to be used in a powertrain model for the purpose of integrated powertrain design optimization. The proposed model can be scaled for the individual components of the organic Rankine cycle and captures the transient behavior by only four thermodynamic states. The model was compared with a finite volume model (Chowdhury et al., 2015). Both models yield similar behavior, however, still differences in time response and steady-state values does exist.

The model was integrated into the simulation model of a parallel hybrid heavy-duty truck. ECMS linked with a Newton-Raphson shooting method, was used to solve the optimal control problem over a drive cycle. Results on the UDDS drive cycle showed more use of the electric machine, the use of higher gears, and a 2.5% improvement in fuel economy (6 % on a more highway type of cycle) when including a WHR in the powertrain. Future work focuses on a more extensive validation of the ORC model, a benchmark with dynamic programming on the optimality of the control approach, and a full powertrain design optimization, including the WHR model.

REFERENCES

Bell, I.H., Quoilin, S., Wronski, J., and Lemort, V. (2013). Coolprop: An open-source reference-quality thermophyscal property library. In *ASME ORC 2nd International Seminar on ORC Power Systems*.

Cellier, F.E. and Kofman, E. (2006). *Continuous system simulation*. Springer Science & Business Media, Berlin.

Chowdhury, J., Nguyen, B., and Thornhill, D. (2015). Modelling of evaporator in waste heat recovery system using finite volume method and fuzzy technique. *Energies*, 8(12), 14078 – 14097.

Feru, E., Murgovski, N., de Jager, A., and Willems, F. (2016). Supervisory control of a heavy-duty Diesel engine with an electrified waste heat recovery system. *Control Engineering Practice*, 54, 190–201.

Guzzella, L. and Sciaretta, A. (2007). *Vehicle propulsion systems*. Springer, Berlin.

Huster, W., Vaupel, Y., Mhamdi, A., and Mitsos, A. (2018). Validated dynamic model of an organic Rankine cycle (orc) for waste heat recovery in a Diesel truck. *Energy*, 151, 647–661.

Lion, S., Michos, C., Vlaskos, I., Rouaud, C., and Taccani, R. (2017a). A review of waste heat recovery and organic Rankine cycles (orc) in on-off highway vehicle heavy duty Diesel engine applications. *Renewable and Sustainable Energy Reviews*, 79, 691–708.

Lion, S., Vlaskos, I., Rouaud, C., and Taccani, R. (2017b). Overview of the activities on heavy duty Diesel engine waste heat recovery with organic Rankine cycle (orc) in the frame of the ecco-mate eu fp7 project. *Energy Procedia*, 129, 786–793.

Maamria, D. (2015). *Dynamic optimization in multi-states systems for automobile energy efficiency*. Ph.D. thesis, Paris Institute of Technology.

Nelson, C. (2008). Exhaust energy recovery. In *Diesel Engine-Efficiency and Emissions Research Conference*, 4–7.

Peralez, J., Tona, P., Lepreux, O., Sciarretta, A., Voise, L., Dufour, P., and Nadri, M. (2013). Improving the control performance of an organic Rankine cycle system for waste heat recovery from a heavy-duty Diesel engine using a model-based approach. In *52nd IEEE Conference on Decision and Control*, 6830–6836.

Petr, P., Tegethoff, W., and Köhler, J. (2017). Method for designing waste heat recovery systems (whrs) in vehicles considering optimal control. *Energy Procedia*, 129, 232–239.

Rosset, K., Mounier, V., Guenat, E., and Schiffman, J. (2018). Multi-objective optimization of turbo-orc systems for waste heat recovery on passenger car engines. *Energy*, 159, 751–765.

Stanton, D.W. (2013). Systematic development of highly efficient and clean engines to meet future commercial vehicle greenhouse gas regulations. *SAE International Journal of Engines*, 6, 1395–1480.

Turns, S.R. (2006). *Thermodynamics: concepts and applications*. Cambridge University Press, Cambridge.

Zhao, R., Zhang, H. Song, S., Tian, Y., Yang, Y., and Liu, L. (2018). Integrated simulation and control strategy of the Diesel engine-organic Rankine cycle (orc) combined system. *Energy Conversion and Management*, 156, 639 – 654.